A new four-dimensional *ab initio* potential energy surface for N_2O–He and vibrational band origin shifts for the N_2O–He_N clusters with $N = 1$–40

Lecheng Wang,[1] Daiqian Xie,[1,a)] Robert J. Le Roy,[2] and Pierre-Nicholas Roy[2,a)]
[1]*Institute of Theoretical and Computational Chemistry, Key Laboratory of Mesoscopic Chemistry, School of Chemistry and Chemical Engineering, Nanjing University, Nanjing 210093, China*
[2]*Department of Chemistry, University of Waterloo, Waterloo, Ontario N2L 3G1, Canada*

(Received 23 July 2012; accepted 17 August 2012; published online 12 September 2012)

A new four-dimensional *ab initio* potential energy surface for N_2O−He is constructed at the CCSD(T) level with an aug-cc-pVQZ basis set together with bond functions. The vibrational coordinates Q_1 and Q_3 of N_2O are explicitly included, due to the strong coupling between the symmetric and asymmetric stretches of N_2O. A global potential energy surface is obtained by fitting the original potential points to a four-dimensional Morse/long range (MLR) analytical form. In the fitting, the *ab initio* noise in the long range region of the potential is smoothed over by theoretically fixed long range parameters. Two-dimensional intermolecular potentials for both the ground and the excited υ_3 states of N_2O are then constructed by vibrationally averaging the four-dimensional potential. Based on the two-dimensional potentials, we use the path integral Monte Carlo algorithm to calculate the vibrational band origin shifts for the N_2O−He_N clusters using a first order perturbation theory estimate. The calculated shifts agree reasonably well with the experimental values and reproduce the evolution tendency from dimer to large clusters. © *2012 American Institute of Physics*. [http://dx.doi.org/10.1063/1.4749248]

I. INTRODUCTION

Ultracold helium clusters doped by small chromophore molecules, such as N_2O, CO_2, OCS, and CO, have been an important theoretical and experimental subject during past decades.[1–13] The observed variations of spectroscopic properties with the size of the clusters offer key insight into the structural and dynamical behaviour in the micro-solvation environment. The turnaround in the evolution of the rotational constant with the number of the helium atoms in the {chromophore}−He_N clusters has been associated with the onset of superfluidity.[1–5,14] McKellar and co-workers[11–13] also found that the size dependence of the shift of the N_2O antisymmetric stretch υ_3 band origin could provide deeper insight into the transition from an impurity-solvent dimer to a doped bulk solution.

Among these doped impurity chromophores, N_2O is distinctive due to the anisotropy of its interaction with helium atoms. Nauta and Miller observed that the rotation of N_2O is much more strongly hindered than that of CO_2 in the ^{4}He nanodroplet, although their gas phase rotational constants are very similar.[14] Later, several groups[1,2,11] recorded more detailed evolutions of the vibrational band origin shift with the helium number, which typically has a turnaround for small clusters, corresponding to the completion of a donut-shaped ring around the middle of the linear N_2O impurity. A similar size dependence was also observed for the rotational constant[11–13] and superfluid response of N_2O embedded in ^{4}He clusters.[1,3,11] Besides, both the vibrational band origin shifts and the rotational constants show a leveling-off behavior for large clusters coinciding to the nano-droplet limit.

To provide quantum mechanical insight into these observations, theoretical simulations based on computed dimer potential energy surfaces (PESs) were performed.[15–19] Earlier theoretical studies for the rovibrational spectra of the N_2O−He complex were performed based on two-dimensional (2D) N_2O−He PESs with fixed internal modes of N_2O.[15–17] While a 2D treatment may be adequate for describing the rotational spectra, it could not properly describe infrared spectra involving excitation of an intramolecular N_2O vibrational mode. The first attempt to take account of the asymmetric stretch coordinate (Q_3) of N_2O was due to Zhou and coworkers, who fixed other internal modes at their equilibrium values.[18] Recently, we constructed a new three-dimensional (3D) PES with an aug-cc-PVQZ basis set by involving the Q_3 mode of N_2O with other internal modes fixed at their averaged values of the corresponding vibrational state.[19] The path integral Monte Carlo (PIMC) simulations based on this PES reproduced the rotational constants accurately. However, the prediction of the shift of the vibrational band origin was not satisfactory. One inadequacy of our previous dimer potential may come from the neglect of the symmetric vibrational coordinate Q_1. Because of the strong coupling of the symmetric and asymmetric stretch modes of the non-symmetric N_2O molecule, neglect of the effect of the Q_1 coordinate in the potential may be an inadequate approximation here, although it was adequate for CO_2−He.[20,21]

In this work, a four-dimensional (4D) PES for N_2O−He is constructed by explicitly including both the symmetric and

a)Authors to whom correspondence should be addressed. Electronic addresses: dqxie@nju.edu.cn and pnroy@uwaterloo.ca.

asymmetric vibrational coordinates of N_2O. The analytical Morse/long-range (MLR) function introduced by Le Roy and co-workers[20] is employed to fit the *ab initio* grids. In this way, the long-range part of the potential energy surface of N_2O−He is fixed to have an appropriate theoretical form, as was done previously for CO_2−He.[21] This smoothes over the noise that arises in the *ab initio* results when the interaction energies are small. Based on the new dimer PES, the PIMC (Refs. 22–24) method developed by Blinov and Roy[21,25] is used to obtain the band origin shifts of the N_2O−He_N clusters. In this version of PIMC method, the rotational degrees of freedom of the impurity are explicitly incorporated.[25,26] Bosonic exchanges of solvent particles are sampled using the worm algorithm.[27,28] In addition, a perturbation based approach[21] is used to accelerate the convergence of the calculation of Δv.

This paper is organized as follows. Section II describes the construction of the smooth 4D N_2O−He dimer PES. Section III summarizes the PIMC approach for simulating doped helium clusters and presents details of the first-order perturbation theory approach to obtain vibrational shifts. Section IV then presents the features of our PES and compares it with an earlier model, and presents the PIMC simulation results. We conclude and summarize in Sec. V.

II. POTENTIAL ENERGY SURFACE

A. *Ab initio* details

The PES is constructed in terms of four coordinates (R, θ, r_{NN}, r_{NO}), where R denotes the distance between He and the center of mass of N_2O and θ denotes the associated Jacobi angle with $\theta = 0^\circ$ corresponding to the linear configuration with the N atom facing the He atom. The two independent bond lengths r_{NN} and r_{NO} are associated with the two vibrational normal coordinates Q_1 and Q_3. A total of 713 N_2O−He dimer geometries (R, θ) are included in our *ab initio* calculations, with 31 R grid points ranging from 2 to 10 Å and 23 angular grid points. These grid points are not evenly distributed, with more points at the well region. Calculations were performed at 30 pairs of intramolecular coordinates (r_{NO}, r_{NN}) for each N_2O−He dimer geometry. The product of the intermolecular and intramolecular grids leads to a total of 21 390 points, which were calculated with the MOLPRO package[29] using single- and double-excitation coupled-cluster theory with a noniterative pertubation treatment of triple excitations [CCSD(T)].[30] The basis set is taken as the augmented correlation-consistent quadruple-zeta (aug-cc-pVQZ) basis set of Woon and Dunning[31] with an additional set of bond functions (3*s*3*p*2*d*1*f*1*g*) (for 3*s* and 3*p*, $\alpha = 0.9$, 0.3, and 0.1; for 2*d*, $\alpha = 0.6$ and 0.2, and for *f*, *g*, $\alpha = 0.3$) (Ref. 32) located at the center of the van der Waals bond. The intermolecular potential $V_{MLR}(r_{NO}, r_{NN}, R, \theta)$, which is defined as the difference between the total energy of the N_2O−He dimer and the sum of the energies of the N_2O and He monomers, is obtained within the supermolecular approach with the correction for basis set superposition error (BSSE) performed by the full counterpoise procedure.[33]

B. Analytical 4D MLR function form

The 4D *ab initio* intermolecular potential points are fitted to a four dimensional Morse/long-range (4D-MLR) analytic form:[20]

$$V_{MLR}(r_{NO}, r_{NN}, R, \theta) = D_e(r_{NO}, r_{NN}, \theta) \times \left[1 - \frac{u_{LR}(r_{NO}, r_{NN}, R, \theta)}{u_{LR}(r_{NO}, r_{NN}, R_e, \theta)} \times e^{-\beta(r_{NO}, r_{NN}, R, \theta) y_p(r_{NO}, r_{NN}, R, \theta)}\right]^2, \quad (1)$$

in which $D_e(r_{NO}, r_{NN}, \theta)$ is the well depth and $R_e = R_e(r_{NO}, r_{NN}, \theta)$ is the position of the minimum on a radial cut through the potential at the angle θ for a particular set of N_2O intramolecular coordinates (r_{NO}, r_{NN}). $u_{LR}(r_{NO}, r_{NN}, R, \theta)$ is a function which defines the (attractive) limiting long-range behavior of the effective 1D potential along that cut as

$$V_{MLR}(r_{NO}, r_{NN}, R, \theta) \approx D_e(r_{NO}, r_{NN}, \theta) - u_{LR}(r_{NO}, r_{NN}, R, \theta). \quad (2)$$

Due to the anisotropy of the N_2O molecule and the nonpolar nature of the He atom, the appropriate functional form for $u_{LR}(r_{NO}, r_{NN}, R, \theta)$ is taken as

$$u_{LR}(r_{NO}, r_{NN}, R, \theta) = \sum_{n=6}^{10} \frac{1}{R^n} \sum_{l=0}^{L_{max}(n)} P_l(\cos\theta) C_n^l(r_{NO}, r_{NN}), \quad (3)$$

in which $C_n^l(r_{NO}, r_{NN})$ are the long range coefficients, and $P_l(\cos\theta)$ is a Legendre polynomial in $\cos\theta$. The $u_{LR}(r_{NO}, r_{NN}, R_e, \theta)$ factor in the denominator of Eq. (1) is the same function evaluated at $R = R_e(r_{NO}, r_{NN}, \theta)$. The choice of long range coefficients is discussed in detail in Subsection II C. The radial variable in the exponent in Eq. (1) is dimensionless and has the form

$$y_p(r_{NO}, r_{NN}, R, \theta) = \frac{R^p - R_e^p(r_{NO}, r_{NN}, \theta)}{R^p + R_e^p(r_{NO}, r_{NN}, \theta)}, \quad (4)$$

where p is a natural number which must be greater than the difference between the largest and the smallest (inverse) power in Eq. (3), $p > 4$. The exponent coefficient function $\beta(r_{NO}, r_{NN}, R, \theta)$ is a fairly slowly varying function of R, which is written as a constrained polynomial,

$$\beta(r_{NO}, r_{NN}, R, \theta) = y_p(r_{NO}, r_{NN}, R, \theta)\beta_\infty(r_{NO}, r_{NN}, \theta) + \lfloor 1 - y_p(r_{NO}, r_{NN}, R, \theta)\rfloor \times \sum_{i=0}^{N_\beta} \beta_i(r_{NO}, r_{NN}, \theta) y_q^i(r_{NO}, r_{NN}, R, \theta). \quad (5)$$

The expansion length of β_i is $N_\beta = 4$. Recently, it has been shown that the use of a separate smaller power $q < p$ to define the radial variable in the power-series portion of Eq. (5) can lead to more compact and robust potential functions.[34] In this work, these values are set to $p = 5$ and $q = 2$.

A key property of this potential function form is the fact that the limiting long-range behavior of $\beta(r_{NO}, r_{NN}, R, \theta)$ implied by the definition of $y_p(r_{NO}, r_{NN}, R, \theta)$ and the algebraic structure of Eqs. (1) and (5) is

$$\lim_{R\to\infty} \beta(r_{NO}, r_{NN}, R, \theta) \equiv \beta_\infty(r_{NO}, r_{NN}, \theta) = \ln \frac{2D_e(r_{NO}, r_{NN}, \theta)}{u_{LR}(r_{NO}, r_{NN}, R_e, \theta)}. \quad (6)$$

The parameters $D_e(r_{NO}, r_{NN}, \theta)$, $R_e(r_{NO}, r_{NN}, \theta)$, and $\beta_i(r_{NO}, r_{NN}, \theta)$ are all represented as polynomials expansions in (r_{NO}, r_{NN}) and Legendre expansions in $\cos\theta$ in our 4D MLR analytical form,

$$A(r_{NO}, r_{NN}, \theta) = \sum_{\lambda=0} P_\lambda(\cos\theta) \sum_{i=0}^{I_{max}} \sum_{j=0}^{J_{max}} A^{\lambda ij} r_{NO}^i r_{NN}^j, \quad (7)$$

where $A = D_e$, R_e, or β_i. The polynomial expansion length is set to $I_{max} = J_{max} = 5$.

C. Smoothing over the *ab initio* calculation noise

The long range coefficients[20,21] are theoretically fixed to smooth over the noise in the original *ab initio* grid points. The leading van der Waals coefficients $C_6^0(r_{NO}, r_{NN})$ and $C_6^2(r_{NO}, r_{NN})$ can be decomposed as $C_6^l(r_{NO}, r_{NN}) = C_{6disp}^l \times (r_{NO}, r_{NN}) + C_{6,ind}^l(r_{NO}, r_{NN})$, where $C_{6,disp}^l(r_{NO}, r_{NN})$ and $C_{6,ind}^l(r_{NO}, r_{NN})$ describe the limiting long range behavior of dispersion and induction energies, respectively. The equilibrium value of the isotropic dispersion term $C_{6,eq,disp}^0$ is calculated from the multipole moments and dynamic polarizabilities of the isolated monomers by Chang and co-workers[15] and its stretching-dependence is defined by that of the spherical average of the polarizability of N_2O,

$$C_{6,disp}^0(r_{NO}, r_{NN}) = C_{6,eq,disp}^0 \left\{ \frac{\bar{\alpha}(r_{NO}, r_{NN})}{\bar{\alpha}_{eq}} \right\}, \quad (8)$$

where $\bar{\alpha}(r_{NO}, r_{NN}) = [\alpha_{//}(r_{NO}, r_{NN}) + 2\alpha_\perp(r_{NO}, r_{NN})]/3$ and $\bar{\alpha}_{eq}$ is its equilibrium value. The leading anisotropic dispersion coefficient $C_{6,disp}^2(r_{NO}, r_{NN})$ is then defined in terms of $C_{6,disp}^0(r_{NO}, r_{NN})$, $\bar{\alpha}(r_{NO}, r_{NN})$, and $\Delta\alpha(r_{NO}, r_{NN}) = \alpha_{//}(r_{NO}, r_{NN}) - \alpha_\perp(r_{NO}, r_{NN})$ of N_2O,

$$C_{6,disp}^2(r_{NO}, r_{NN}) = C_{6,disp}^0(r_{NO}, r_{NN}) \left\{ \frac{\Delta\alpha(r_{NO}, r_{NN})}{3\bar{\alpha}(r_{NO}, r_{NN})} \right\}. \quad (9)$$

The values of all of the other $C_n^l(r_{NO}, r_{NN})$ coefficients for $n = 7$–10 are defined by the product of their equilibrium values from Ref. 15 times the ratio of the stretching-dependent C_6^0 of Eq. (8) to its equilibrium value.

The values of $\alpha_{//}(r_{NO}, r_{NN})$ and $\alpha_\perp(r_{NO}, r_{NN})$ were obtained from *ab initio* calculations with the finite field method. Cubic spline interpolation was used to obtain a polarizability surface from the *ab initio* grid points. The theoretical polarizabilities at the equilibrium geometry of N_2O obtained with our polarizability surface are $\alpha_{//} = 32.501$ and $\alpha_\perp = 13.2455$ (a.u.), which are in good agreement with the experimental values $\alpha_{//} = 32.433$ and $\alpha_\perp = 13.334$.[35]

The induction term $C_{6,ind}^l$ can be approximated as

$$C_{6,ind}^l(r_{NO}, r_{NN}) = [\mu_{N_2O}(r_{NO}, r_{NN})]^2 \alpha_{He}, \quad (10)$$

in which $\mu_{N_2O}(r_{NO}, r_{NN})$ is the stretching-dependent N_2O dipole moment and α_{He} is the polarizability of the atomic He. Due to the small value of dipole moment of the N_2O molecule, 0.0633 a.u.,[36] the induction coefficient is negligibly small and thus the leading long range term C_6^l is dominated by dispersion. Consequently, the induction terms are omitted from our model for the PES.

D. Least-squares fits

Realistic initial trial values of the fitting parameters are essential to any nonlinear least-square fit, and they are obtained as follows in the present fit to determine the 4D-MLR analytical form. At first, the intramolecular vibrational coordinates pairs (r_{NO}, r_{NN}) are held fixed and the 713 (R, θ) grid points for each of the 30 fixed pairs are fitted to a 2D version of the MLR form[20] to extract the stretching-dependent parameters $D_e^\lambda(r_{NO}, r_{NN})$, $R_e^\lambda(r_{NO}, r_{NN})$, and $\beta_i^\lambda(r_{NO}, r_{NN})$ of the 2D function:

$$V_{MLR}(R, \theta) = D_e(\theta) \times \left[1 - \frac{u_{LR}(R, \theta)}{u_{LR}(, R_e, \theta)} e^{-\beta(R,\theta) y_p(R,\theta)} \right]^2. \quad (11)$$

The resulting parameter values are then fitted to polynomial expansions in (r_{NO}, r_{NN})

$$A^\lambda(r_{NO}, r_{NN}) = \sum_{i=0}^{5} \sum_{j=0}^{5} A^{\lambda ij} r_{NO}^i r_{NN}^j, \quad (12)$$

where $A = D_e$, R_e, or β_i, and the resulting values of $A^{\lambda ij}$ are used as the starting parameters in the global 4D-MLR fit to Eq. (1). In the 4D-MLR fits, the input *ab initio* energies are weighted by uncertainties assigned to $u_i = 0.1$ cm^{-1} for the attractive region where $V(r_{NO}, r_{NN}, R, \theta) \le 0.0$ cm^{-1}, while for the repulsive wall region $u_i = [V(r_{NO}, r_{NN}, R, \theta) + 1.0]/10.0$. The sequential rounding and refitting procedure[37] are used to fix the parameters with small contribution to zero. Finally, 592 parameters are used to fit the 21 390 *ab initio* points, yielding a root mean square residual discrepancy of 0.763 cm^{-1} for points with energy lower than 1000 cm^{-1}. Almost half (258/592) of these fitting parameters are used to define $D_e(r_{NO}, r_{NN}, \theta)$, about one third (182/592) are required to define $R_e^p(r_{NO}, r_{NN}, \theta)$, and 62, 40, 17, 22, 11 to define $\beta_i(r_{NO}, r_{NN}, \theta)$ for $i = 0$–4, respectively. The list of the 21 390 *ab initio* points, the resulting set of potential parameters and a FORTRAN subroutine for generating these potentials may be obtained from the supplementary material.[38]

E. Vibrational-averaged 2D PES

The 2D dimer PES $V(R, \theta)$ of N_2O–He is obtained by averaging over the intramolecular coordinates (r_{NO}, r_{NN}) in our original 4D PES $V(r_{NO}, r_{NN}, R, \theta)$ with appropriate vibrational wavefunctions of the N_2O monomer,

$$V^{v_3}(R, \theta) = \langle \psi^{v_3}(r_{NO}, r_{NN}) | V(r_{NO}, r_{NN}, R, \theta) \times | \psi^{v_3}(r_{NO}, r_{NN}) \rangle, \quad (13)$$

TABLE I. Parameters D_e^λ, R_e^λ, and β_i^λ of 2D MLR analytical form for the vibrational ground state of N_2O. D_e^λ in cm^{-1} and R_e^λ in Å.

D_e^0	34.236	D_e^{10}	− 3.8	R_e^1	0.1521	R_e^{11}	− 0.0054	β_0^6	− 0.068	β_2^0	− 0.32
D_e^1	− 0.3299	D_e^{11}	1.75	R_e^2	0.9496	R_e^{12}	0.0053	β_0^7	− 0.008	β_2^1	− 0.65
D_e^2	21.349	D_e^{12}	1.77	R_e^3	0.0165	R_e^{13}	0.0009	β_0^8	0.045	β_2^2	0.26
D_e^3	0.53	D_e^{13}	− 1.1	R_e^4	− 0.3549	R_e^{14}	− 0.0041	β_1^0	0.228	β_2^3	0.03
D_e^4	22.12	D_e^{14}	− 0.7	R_e^5	0.0596	β_0^0	− 0.1974	β_1^1	− 0.217	β_2^4	− 0.05
D_e^5	− 4.54	D_e^{15}	0.58	R_e^6	0.1245	β_0^1	0.113	β_1^2	0.279	β_3^0	0.57
D_e^6	− 12.88	D_e^{16}	0.23	R_e^7	− 0.0309	β_0^2	0.329	β_1^3	0.05	β_3^1	− 1.1
D_e^7	3.09	D_e^{17}	− 0.18	R_e^8	− 0.0417	β_0^3	− 0.002	β_1^4	− 0.05	β_3^2	0.4
D_e^8	7.73	D_e^{18}	− 0.05	R_e^9	0.0172	β_0^4	0.074	β_1^5	− 0.05	β_4^0	− 0.3
D_e^9	− 2.67	R_e^0	3.63301	R_e^{10}	0.0039	β_0^5	0.017	β_1^6	− 0.05		

where $\psi^{\upsilon_3}(r_{NO}, r_{NN})$ is the vibrational wave function with vibrational state $\upsilon_3 = 0$ and 1. The 2D vibrational averaged surface was then fitted to the 2D MLR form as Eq. (11). Compared with the previous 4D version, the parameters $A(r_{NO}, r_{NN}, \theta)$, for $A = D_e$, R_e, or β_i are replaced by $\bar{A}(\theta)$, where

$$\bar{A}(\theta) = \sum_{\lambda=0} \bar{A}^\lambda P^\lambda(\cos\theta). \tag{14}$$

Again, the long range parameters are fixed to the theoretical values. For the vibrational ground state, these parameters are directly taken from Chang and co-workers.[15] The leading terms for the excited state are scaled by the vibrational averaged polarizability obtained from the *ab initio* polarizability surface in Subsection II C,

$$\bar{C}_6^{0,\upsilon_3=1} = \bar{C}_6^{0,\upsilon_3=0} \left\{ \frac{\langle\bar{\alpha}\rangle^{\upsilon_3=1}}{\langle\bar{\alpha}\rangle^{\upsilon_3=0}} \right\} \text{ and}$$
$$\bar{C}_6^{2,\upsilon_3=1} = \bar{C}_6^{2,\upsilon_3=0} \left\{ \frac{\langle\Delta\alpha\rangle^{\upsilon_3=1}}{\langle\Delta\alpha\rangle^{\upsilon_3=0}} \right\}. \tag{15}$$

The calculated values of the terms in the left of Eq. (15) is 78341.26 Å^6 cm^{-1} and 23765.75 Å^6 cm^{-1}, correspondingly. The parameters of the fits of the υ_3 ground and excited states PESs are shown in Tables I and II respectively. For both ground and excited state PESs, only 59 fitting parameters are required to yield a standard error 0.027 cm^{-1}. The FORTRAN subroutine for generating these potentials may be obtained from the supplementary material.[38]

III. PATH INTEGRAL MONTE CARLO METHOD

A. Hamiltonian

The total Hamiltonian for the N_2O−He_N clusters is presented as

$$\hat{H} = \hat{H}_{He} + \hat{H}_{N_2O} + V_{N_2O-He_N}. \tag{16}$$

The Hamiltonian for helium atoms is given in terms of the momenta $\mathbf{p}_i$ and positions $\mathbf{r}_i$ of the ith helium atom, and a pairwise potential u between two helium atoms based on that of Aziz and co-workers,[39]

$$\hat{H}_{He} = \sum_{i=1}^{N} \frac{\mathbf{p}_i^2}{2m_{He}} + \sum_{i<j} u(|\mathbf{r}_i - \mathbf{r}_j|). \tag{17}$$

The Hamiltonian for the N_2O dopant contains translations and rotations,

$$\hat{H}_{N_2O} = \frac{\mathbf{p}_0^2}{2m_{N_2O}} + B_{N_2O}\mathbf{L}^2, \tag{18}$$

where $\mathbf{p}_0$ and $\mathbf{L}$ are the linear momentum and rotational angular momenta of the N_2O molecule respectively. The rotational constant $B_{N_2O}^{\upsilon_3}$ depends on the vibrational state with values of $B_{N_2O}^{\upsilon_3=0} = 0.4190110\,cm^{-1}$ and $B_{N_2O}^{\upsilon_3=1} = 0.4155565\,cm^{-1}$ for the ground[40] and excited[41] states respectively. The total interaction potential between N_2O and He is given in a pairwise additive form in terms of the Jacobi coordinates R_i and θ_i of the ith helium atom with respect to the N_2O impurity,

$$V_{N_2O-He_N} = \sum_i V_{N_2O-He}(R_i, \theta_i). \tag{19}$$

TABLE II. Parameters D_e^λ, R_e^λ, and β_i^λ of 2D MLR analytical form for the vibrational state $\upsilon_3 = 1$ of N_2O. D_e^λ in cm^{-1} and R_e^λ in Å.

D_e^0	34.801	D_e^{10}	− 3.65	R_e^1	0.1531	R_e^{11}	− 0.0052	β_0^6	− 0.067	β_2^0	− 0.34
D_e^1	− 0.334	D_e^{11}	1.75	R_e^2	0.9476	R_e^{12}	0.0054	β_0^7	− 0.008	β_2^1	− 0.64
D_e^2	− 20.924	D_e^{12}	1.7	R_e^3	0.0143	R_e^{13}	0.0008	β_0^8	0.046	β_2^2	0.27
D_e^3	0.61	D_e^{13}	− 1.09	R_e^4	− 0.3536	R_e^{14}	− 0.004	β_1^0	0.225	β_2^3	0.04
D_e^4	21.8	D_e^{14}	− 0.67	R_e^5	0.0614	β_0^0	− 0.197	β_1^1	− 0.217	β_2^4	− 0.05
D_e^5	− 4.63	D_e^{15}	0.58	R_e^6	0.1222	β_0^1	0.113	β_1^2	0.271	β_3^0	0.61
D_e^6	− 21.54	D_e^{16}	0.21	R_e^7	− 0.0312	β_0^2	0.328	β_1^3	0.04	β_3^1	− 1.1
D_e^7	3.12	D_e^{17}	− 0.18	R_e^8	− 0.0411	β_0^3	− 0.003	β_1^4	− 0.04	β_3^2	0.5
D_e^8	7.52	D_e^{18}	− 0.04	R_e^9	0.0172	β_0^4	0.075	β_1^5	− 0.04	β_4^0	− 0.2
D_e^9	− 2.68	R_e^0	3.6367	R_e^{10}	0.0036	β_0^5	0.017	β_1^6	0.02		

B. Path integral Monte Carlo simulations

Given $\beta = 1/k_B T$ and the elements of the density matrix $\hat{\rho} = e^{-\beta \hat{H}}$, the canonical average of a quantum mechanical operator ($\hat{O}$) could be obtained as follows:[23]

$$\langle \hat{O} \rangle_\beta = \frac{1}{Z} \mathrm{Tr}\{\hat{O}\hat{\rho}(\beta)\} = \frac{1}{Z} \int d\mathbf{q} d\mathbf{q}' d\mathbf{\Omega} d\mathbf{\Omega}' \langle \mathbf{q}\Omega | \hat{O} | \mathbf{q}'\mathbf{\Omega}' \rangle \langle \mathbf{q}'\mathbf{\Omega}' | \hat{\rho}(\boldsymbol{\beta}) | \mathbf{q}\mathbf{\Omega} \rangle, \tag{20}$$

where $Z = \mathrm{Tr}\{\hat{\rho}(\beta)\}$ is the partition function, $\mathbf{q} = (\mathbf{r}_0, \{\mathbf{r}_{i>0}\})$ is the set of the translational coordinates of both N_2O and He, and $\mathbf{\Omega}$ denotes the orientation of N_2O in the space-fixed frame.

The finite-temperature PIMC code with the rotation of dopant and the bosonic exchanges of ^{4}He developed by Blinov and Roy[25,26] was used to compute the density matrix and obtain canonical averages. The integral in Eq. (20) is discretized in imaginary time,

$$\langle \mathbf{q}'\Omega' | e^{-\beta \hat{H}} | \mathbf{q}\Omega \rangle = \int \cdots \int \prod_{k=2}^{K'} d\Omega_k \prod_{k=2}^{K} d\mathbf{q}_k \times \prod_{k=1}^{K'} \langle \Omega_k | e^{-\tau' \hat{T}^{\mathrm{rot}}_{N_2O}} | \Omega_{k+1} \rangle \times \prod_{k=1}^{K} \langle \mathbf{q}_k | e^{-\tau \hat{H}^{\mathrm{tr}}} | \mathbf{q}_{k+1} \rangle, \tag{21}$$

where $\hat{T}^{\mathrm{rot}}_{N_2O}$ is the rotational kinetic energy operator of N_2O, and $\hat{H}^{\mathrm{tr}} = \hat{H}_{\mathrm{He}} + \hat{T}^{\mathrm{tr}}_{N_2O} + V_{N_2O-He_N}$ represents the remainder of the Hamiltonian in Eq. (16). The following boundary conditions are used in Eq. (21): $(\mathbf{q}_1\mathbf{\Omega}_1) = (\mathbf{q}'\mathbf{\Omega}')$ and $(\mathbf{q}_{K'+1}\mathbf{\Omega}_{K'+1}) = (\mathbf{q}\mathbf{\Omega})$. The translational and rotational degrees of freedom are sampled separately with different Trotter time slice $\tau = \beta/K$ for translation and $\tau' = \beta/K'$ for rotation.[25] For the evaluation of the density matrix, the primitive approximation[23] is used for the translational degrees of freedom, and a closed form for a linear rotor[42] is used for rotations. In addition, a multilevel Metropolis algorithm[23] is used for the translational degrees of freedom, while the standard Metropolis algorithm is used in sampling the rotational degrees of freedom.[42] The boson exchange is handled in PIMC simulations by the efficient worm algorithm.[27,28]

The vibrational frequency of the N_2O molecule will be shifted when embedded in low temperature helium clusters. The value of the vibrational band origin in such clusters, relative to the free N_2O is evaluated as follows:

$$\Delta\nu^N = \Delta E^{N_2O}_{\mathrm{cluster}} - \Delta E^{N_2O}_{\mathrm{free}} = \bar{E}^N_{\upsilon_3=1} - \bar{E}^N_{\upsilon_3=0}, \tag{22}$$

where $\Delta E^{N_2O}_{\mathrm{cluster}}$ and $\Delta E^{N_2O}_{\mathrm{free}}$ are the transition frequency between vibrational state $\upsilon_3 = 0$ and 1 of N_2O solved in helium clusters and of a free N_2O molecule, respectively, and $\bar{E}^N_{\upsilon_3}$ is the energy of a cluster in the vibrational state υ_3 of N_2O at temperature T. However, the small value of $\Delta\nu^N_0$, compared with $\bar{E}^{[N]}_{\upsilon_3}$ makes PIMC simulations exceedingly difficult to converge for large clusters. Recently, a more efficient approach based on perturbation theory was proposed by Li and co-workers[21,43] The Hamiltonian of the excited vibrational state for N_2O-He_N system can be written as follows:

$$\hat{H}^{\upsilon_3=1} = \hat{H}^{\upsilon_3=0} + \hat{T}^{\upsilon_3=0}_{\mathrm{rot},N_2O} \left\{ \frac{B^{\upsilon_3=1}_{N_2O}}{B^{\upsilon_3=0}_{N_2O}} - 1 \right\} + \hat{V}^{\upsilon_3=1}_{N_2O-He_N} - \hat{V}^{\upsilon_3=0}_{N_2O-He_N}. \tag{23}$$

The quantitative difference between the rotational constants of N_2O between $\upsilon_3 = 0$ and 1 is extremely small. The contribution of the second term in the above Hamiltonian is on the order of 10^{-3} cm^{-1}. Its effect on the band origin shift is negligible. Consequently, we have

$$\hat{H}^{\upsilon_3=1} = \hat{H}^{\upsilon_3=0} + \Delta\hat{V}_{N_2O-He_N}, \tag{24}$$

where $\Delta\hat{V}_{N_2O-He_N} = \hat{V}^{\upsilon_3=1}_{N_2O-He_N} - \hat{V}^{\upsilon_3=0}_{N_2O-He_N}$. Thus first-order perturbation theory yields

$$\Delta\upsilon_N = \langle \Delta V_{N_2O-He_N} \rangle. \tag{25}$$

The above quantity depends on the density distribution of the solvent atoms in the cluster. Denoting the normalized distribution of helium by $\rho(R, \theta)$, the band origin shift can be calculated as

$$\Delta\upsilon_N = \iint d\theta dR \rho(R,\theta) \Delta V_{N_2O-He}(R,\theta). \tag{26}$$

This approach avoids the sampling over kinetic energy operators, resulting in less fluctuation and much faster Monte Carlo convergence.[21]

IV. RESULTS AND DISCUSSION

A. Potential energy surface

A contour plot of N_2O-He dimer PES for the N_2O vibrational ground state is presented in Fig. 1. The plot for the excited state $\upsilon_3 = 1$ is very similar and thus is not given here. For the ground state PES, a T-shaped global minimum is located at $R = 2.965$ Å and $\theta = 92.52°$. The well depth for the

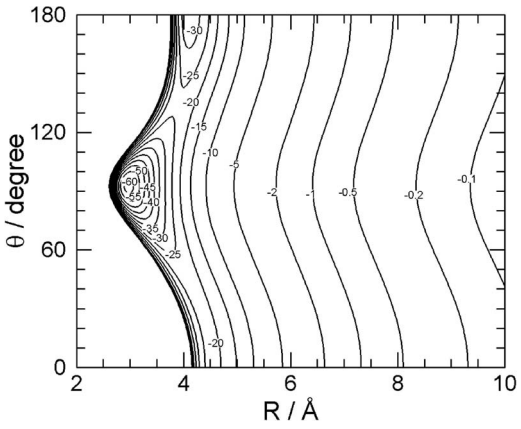

FIG. 1. Contour plot of the fitted vibrational averaged 2D N_2O-He dimer PES (for $\upsilon_3 = 0$). The angles $\theta = 0$ and π correspond to the nitrogen and oxygen ends of the impurity respectively. The energy is in cm^{-1}.

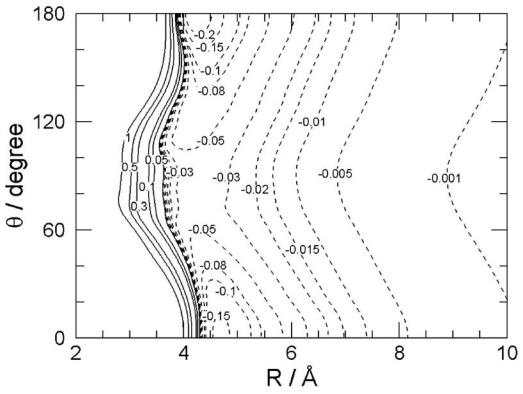

FIG. 2. Contour plot of the potential difference $\hat{V}^{\upsilon_3=1}_{N_2O-He} - \hat{V}^{\upsilon_3=0}_{N_2O-He}$ (in cm^{-1}) between the two averaged intermolecular PESs for the vibrational ground ($\upsilon_3 = 0$) and excited state ($\upsilon_3 = 1$) of CO_2. The angles $\theta = 0$andπ correspond to the nitrogen and oxygen ends of the impurity respectively.

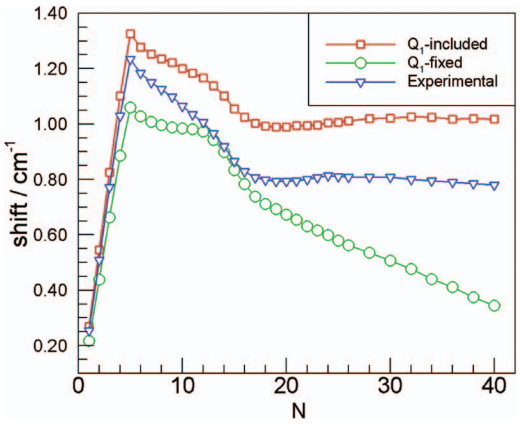

FIG. 3. Vibrational band origin shift calculated by current (red square) PESs compared to the values obtained by previous (green circle) PESs, and experimental observations (blue delta).

vibrational ground state (–61.70 cm^{-1}) is slightly deeper than that for the excited state (–61.03 cm^{-1}). Moreover, a collinear minimum appears at $R = 4.106$ Å, with He attached to the oxygen end of N_2O. Its depth for the ground vibrational state (–33.15 cm^{-1}) is slightly greater than that of the excited state (–33.37 cm^{-1}).

As indicated by Eq. (26), the potential difference $\Delta V_{N_2O-He}(R, \theta)$ is critical for the determination of the vibrational band origin shift. Its contour plot is displayed in Fig. 2. The positive value of potential difference in the T-shaped region will tend to lead to a blueshift of the υ_3 band for small clusters in which the He atoms are all located in a ring around the middle of the N_2O. In contrast, the potential difference at the two ends of doped N_2O is negative, which implies a redshift of the υ_3 band for intermediate-sized clusters for which an increasing fraction of the He atoms lie at larger R values and closer to one of the ends of the molecule. The very small magnitude of the potential difference at long range suggests that the vibrational band origin shift of large clusters should approach a limited value.

The band origin shift $\Delta\upsilon$ for the N_2O-He dimer obtained from pure vdW vibrational bound state calculations is found to be 0.234 cm^{-1}, which is in better agreement with the experimental value[11] of 0.253 cm^{-1} than the value obtained with previous Q_1-fixed N_2O-He PES (Ref. 19) (0.187 cm^{-1}). This improvement confirms the necessity of the inclusion of both symmetric and asymmetric stretch coordinates in the construction of the PESs. In addition, the IR transition frequencies for the N_2O-He dimer are also calculated. The RMS error between the calculated and observed[1] transition frequencies is found to be 0.006 cm^{-1}, which is similar to the results[19] obtained from our previous Q_1-fixed potential and validates the accuracy of this new potential.

B. Vibrational band origin shift for the N_2O-He_N clusters

The evolution of $\Delta\upsilon_N$ with the helium number N for the N_2O-He_N clusters is obtained at 0.37 K with the PIMC methodology, described in Sec. III B. 512 translational and 128 rotational time slices are used to converge the results as tested in our previous study.[19] Simulated values of $\Delta\upsilon_N$ obtained using both Q_1-included and Q_1-fixed version of N_2O-He dimer surface are presented in Fig. 3 together with the experimental data.[11] The listing of the calculated frequency shifts shown in Fig. 3 may be obtained from the supplementary material.[38] The statistical errors are on the order of 10^{-4} cm^{-1}, thus the error bars for the data are smaller than the symbols and are not shown here. The distribution $\rho(R, \theta)$ of the helium atoms around N_2O is not significantly affected by bosonic exchange, thus the effect of bosonic exchange on the vibrational band origin shift is small, although this effect is critical for the simulation of the superfluid ^{4}He clusters.

From Fig. 3, one can see that the calculated band origin shifts using the previous Q_1-fixed potential have significant deviations from the observations, for example, the calculated shifts increase more slowly below $N = 5$, have a kink for medium size clusters at about $N = 12$, and decrease monotonically for larger clusters ($N > 17$). In contrast, the shape of the N-dependence of the calculated band origin shifts based on our new potential is in remarkably good agreement with the observed values with a small systematic discrepancy for larger clusters, which should be due to the error in the PES, or to our neglect of the effect of the υ_2 bending coordinate.

Figure 3 shows that there is a monotonic and almost linear increase in the band origin shifts below $N = 5$, which can be attributed to the formation of the five-membered donut ring.[19] This configuration is a consequence of the deep T-shaped potential minimum of the dimer potential. A sharp turnaround takes place between $N = 5$ and 6, due to occupancy at the oxygen side by additional heliums as presented in our previous work.[19] Afterwards, $\Delta\upsilon_N$ decreases with N until $N > 17$, when the calculated band origin shift levels off. In the large cluster limit, the behavior of our predicted shift is consistent with experimental observation.

The evolution of the band origin shift with cluster size has been discussed before for the CO_2-He_N system.[21,44] The initial blueshift can be understood from the cluster structure. For $N < 6$, the donut ring along the N_2O equator renders the oscillator more stiff, increasing the effective force constant

and leading to blueshifts. Additional helium atoms, particularly those around the O and N termini, increase the effective mass of the oscillator, leading to redshifts. For larger clusters, the additional helium atoms are located at a larger distance, where the difference potential ΔV decreases to have a tiny magnitude. This is why the shift tends to plateau beyond the completion of the first solvation shell.

V. CONCLUSION

We present a new analytic 4D PES for the N_2O-He complex which explicitly incorporates the dependence of the interaction energy on both the Q_1 and Q_3 normal-mode coordinates of N_2O. The *ab initio* interaction energies are obtained at the CCSD(T) level with a large basis set including bond functions located at the midpoint of the intermolecular axis. These *ab initio* grid points are then fitted to a 4D generation of the Morse/long range analytical form with correct theoretically fixed long-range inverse-power behavior, which is critical for a good description of a N_2O molecule doped in medium to large sized He_N clusters. Analogous 2D-MLR potential energy surfaces for the N_2O-He dimer in its ground and υ_3 excited states are obtained by averaging this 4D surface over the asymmetric stretch vibrational wavefunction of N_2O. A finite temperature PIMC study of the vibrational band origin shifts of a rotating N_2O molecule embedded in the $(^4He)_N$ clusters with $N \leq 40$ is then carried out, based on the vibratonal averaged PESs. First-order perturbation theory is used to estimate the vibrational shifts. This approach leads to a statistical estimate with low variance. The calculated vibrational band origin shifts are in much better agreement with the known experimental values than the results from the previous Q_1-fixed PES. In particular, the large cluster limit of the vibrational band origin shift is correctly reproduced in the present simulations. The new PESs should provide a reliable platform for further theoretical studies on the structural and spectroscopic properties of these important clusters.

ACKNOWLEDGMENTS

L.W. and D.X. were supported by the National Natural Science Foundation of China (21133006 and 91021010). R.J.L. and P.N.R. acknowledge Natural Sciences and Engineering Research Council of Canada (NSERC), the Canada Foundation for Innovation (CFI), the University of Waterloo, and the Shared Hierarchical Academic Research Computing Network (SHARCNET) for computing time.

[1] J. Tang and A. R. W. McKellar, J. Chem. Phys. **117**, 2586 (2002).
[2] Y. J. Xu, W. Jäger, J. Tang, and A. R. W. McKellar, Phys. Rev. Lett. **91**, 163401 (2003).
[3] Y. J. Xu, N. Blinov, W. Jäger, and P.-N. Roy, J. Chem. Phys. **124**, 081101 (2006).
[4] Y. J. Xu and W. Jäger, J. Chem. Phys. **119**, 5457 (2003).
[5] J. Tang, A. R. W. McKellar, F. Mezzacapo, and S. Moroni, Phys. Rev. Lett. **92**, 145503 (2004).
[6] J. Tang and A. R. W. McKellar, J. Chem. Phys. **119**, 754 (2003).
[7] J. Tang and A. R. W. McKellar, J. Chem. Phys. **119**, 5467 (2003).
[8] J. Tang and A. R. W. McKellar, J. Chem. Phys. **121**, 181 (2004).
[9] F. Paesani, Y. Kwon, and K. B. Whaley, Phys. Rev. Lett. **94**, 153401 (2005).
[10] A. R. W. McKellar, Y. J. Xu, and W. Jäger, Phys. Rev. Lett. **97**, 183401 (2006).
[11] A. R. W. McKellar, J. Chem. Phys. **127**, 044315 (2007).
[12] A. R. W. McKellar, Y. J. Xu, and W. Jäger, J. Phys. Chem. A **111**, 7329 (2007).
[13] A. R. W. McKellar, J. Chem. Phys. **128**, 044308 (2008).
[14] K. Nauta and R. E. Miller, J. Chem. Phys. **115**, 10254 (2001).
[15] B. T. Chang, O. Akin-Ojo, R. Bukowski, and K. Szalewicz, J. Chem. Phys. **119**, 11654 (2003).
[16] F. Paesani and K. B. Whaley, J. Chem. Phys. **121**, 5293 (2004).
[17] Y. Z. Zhou and D. Q. Xie, J. Chem. Phys. **120**, 8575 (2004).
[18] Y. Z. Zhou, D. Q. Xie, and D. H. Zhang, J. Chem. Phys. **124**, 144317 (2006).
[19] L. Wang, D. Xie, H. Guo, H. Li, P.-N. Roy, and R. J. Le Roy, J. Mol. Spectrosc. **267**, 136 (2011).
[20] H. Li and R. J. Le Roy, Phys. Chem. Chem. Phys. **10**, 4128 (2008).
[21] H. Li, N. Blinov, P.-N. Roy, and R. J. Le Roy, J. Chem. Phys. **130**, 144305 (2009).
[22] Y. Kwon and K. B. Whaley, J. Chem. Phys. **115**, 10146 (2001).
[23] D. M. Ceperley, Rev. Mod. Phys. **67**, 279 (1995).
[24] E. W. Draeger and D. M. Ceperley, Phys. Rev. Lett. **90**, 065301 (2003).
[25] N. Blinov, X. Song, and P.-N. Roy, J. Chem. Phys. **120**, 5916 (2004).
[26] N. Blinov and P.-N. Roy, J. Low Temp. Phys. **140**, 253 (2005).
[27] M. Boninsegni, N. V. Prokof' ev, and B. V. Svistunov, Phys. Rev. E **74**, 036701 (2006).
[28] M. Boninsegni, N. V. Prokof' ev, and B. V. Svistunov, Phys. Rev. Lett. **96**, 070601 (2006).
[29] H.-J. Werner, P. J. Knowles, R. Lindh, F. R. Manby, M. Schütz *et al.*, MOLPRO, version 2006.1, a package of *ab initio* programs, 2006, see http://www.molpro.net.
[30] K. Raghavachari, G. W. Trucks, J. A. Pople, and M. Head-Gordon, Chem. Phys. Lett. **157**, 479 (1989).
[31] D. E. Woon and T. H. Dunning, J. Chem. Phys. **98**, 1358 (1993).
[32] T. B. Pedersen, B. Fernandez, H. Koch, and J. Makarewicz, J. Chem. Phys. **115**, 8431 (2001).
[33] S. F. Boys and F. Bernardi, Mol. Phys. **19**, 553 (1970).
[34] R. J. Le Roy, N. S. Dattani, J. A. Coxon, A. J. Ross, P. Crozet, and C. Linton, J. Chem. Phys. **131**, 204309 (2009).
[35] U. Hohm, Chem. Phys. **179**, 533 (1994).
[36] J. M. L. J. Reinartz, W. L. Meerts, and A. Dymanus, Chem. Phys. **31**, 19 (1978).
[37] R. J. Le Roy, J. Mol. Spectrosc. **191**, 223 (1998).
[38] See supplementary material at http://dx.doi.org/10.1063/1.4749248 for ASCII files containing listings of the *ab initio* energies and of the parameters defining our new 4D potential energy surface for N_2O–He, for FORTRAN subroutines for generating those 4D and vibrationally averaged 2D potentials for $\upsilon_3 = 0$ and 1, and for a listing of the calculated frequency shifts shown in Fig. 3.
[39] R. A. Aziz, A. R. Janzen, and M. R. Moldover, Phys. Rev. Lett. **74**, 1586 (1995).
[40] R. A. Toth, J. Opt. Soc. Am. B **4**, 357 (1987).
[41] M. Kobayashi and I. Suzuki, J. Mol. Spectrosc. **125**, 24 (1987).
[42] D. Marx and M. H. Huser, J. Phys.: Condens. Matter **11**, R117 (1999).
[43] R. J. Le Roy, M. R. Davies, and M. E. Lam, J. Phys. Chem. **95**, 2167 (1991).
[44] Z. Li, L. C. Wang, H. Ran, D. Q. Xie, N. Blinov, P.-N. Roy, and H. Guo, J. Chem. Phys. **128**, 224513 (2008).